Generation of flat-laser Compton scattering γ-ray beam

Hideaki Ohgaki,[1,*] Khaled Ali,[1,†] Toshiteru Kii,[1] Heishun Zen,[1] Takehito Hayakawa,[2,3] Toshiyuki Shizuma,[2] Masaki Fujimoto,[4] and Yoshitaka Taira[4]

[1]*Institute of Advanced Energy, Kyoto University, Gokasho, Uji, Kyoto 611-0011, Japan*
[2]*Kansai Photon Science Institute, National Institutes for Quantum Science and Technology, Kizugawa, Kyoto 619-0215, Japan*
[3]*Institute of Laser Engineering, Osaka University, Suita 565-0871, Japan*
[4]*UVSOR-III Synchrotron Facility, Institute for Molecular Science, National Institutes of Natural Sciences, Okazaki 444-8585, Japan*

(Received 24 January 2023; accepted 31 July 2023; published 22 September 2023)

To develop an isotope selective computed tomography imaging technique, a flat-laser Compton scattering γ-ray beam (F-LCS) by using a helical undulator installed in a storage ring has been proposed. An LCS beam with a broad energy spectrum and spatial distribution, keeping a small beam size, is preferable for multi-isotope imaging and qualitative evaluation. EGS5 simulations assuming the BL1U beamline in UVSOR have been carried out and the result shows that the energy bandwidth of the LCS beam is widened from 2.7% to 22% (FWHM) with a beam size of 2 mm in diameter by varying the undulator K value from 0 to 0.4. A proof of principle (POP) experiment has been carried out in the BL1U, where the APPLE-II undulator has been installed. The K value dependency of the energy spectrum of the generated LCS beam was measured. As a result, a broader energy bandwidth of the LCS beam was observed as the undulator K value increased. The measured energy spectra agreed with the EGS5 results.

DOI: 10.1103/PhysRevAccelBeams.26.093402

I. INTRODUCTION

Tunable monochromatic γ-ray beams have been generated by laser Compton scattering (LCS) in various facilities [1–6]. One of the remarkable applications using LCS beams is a nondestructive analysis of hidden materials through nuclear resonance fluorescence (NRF) [7–13]. So far, we have successfully demonstrated a three-dimensional (3D) isotope-selective computed tomography image of a sample consisting of enriched ^{208}Pb and ^{206}Pb rods using NRF [14] induced by an LCS beam. To obtain high-resolution images, a small size of an incident LCS beam is indispensable, which makes a narrow bandwidth of the LCS energy spectrum. However, a narrow bandwidth LCS beam is difficult to excite multiple isotopes in one-time measurement. Therefore, in our previous measurement [15] where NRF levels of ^{14}N (4.915 MeV) and ^{12}C (4.439 MeV) were excited at the same time, and an 8-mmφ collimator was employed to generate about 20% bandwidth of the LCS beam. In addition, the LCS interaction has a scattering angle dependence in the energy of the scattered γ ray that makes the LCS beam have a spatial dependency in the energy distribution. Therefore, it is difficult to quantitatively evaluate NRF yields in a sample by using standard LCS beams. A flat-laser Compton scattering γ-ray (F-LCS) beam with a broad peak and flat spatial distribution in the energy spectrum has been studied to obtain a multiple isotopes CT Imaging with a high spatial resolution enabling a quantitative evaluation of measured isotopes using a small LCS beam size.

We have proposed the F-LCS beam which has broader energy bandwidth with a small beam size and a spatially uniform energy spectrum. By using a helical undulator installed in a storage ring, such as the APPLE-II undulator in the BL1U beamline of the UVSOR synchrotron facility [16], a circular motion of electrons stored in the storage ring can be excited. This circular motion of electrons widens the electron beam size and divergence. Due to the LCS interaction principle, broader bandwidth and a wider spatial distribution of the scattered γ-ray beam can be expected. In this paper, we describe the concept of the generation of the F-LCS beam, a modeling of simulation with EGS5 [17], and its result. We also report our proof-of-principle (POP) experiment carried out in the BL1U of UVSOR and the comparison with the EGS5 simulation.

*Corresponding author: ohgaki.hideaki.2w@kyoto-u.ac.jp
†Present address: Faculty of Science, South Valley University, 83523 Qena, Arab Republic of Egypt.

II. PRINCIPLE OF F-LCS BEAM GENERATION

Collision between a relativistic electron beam and an intense laser beam generates an LCS beam [18]. The scattered laser photon, whose energy is E_p, with a scattered angle of θ_γ has an energy dependency as described in the following formula [18]:

$$E_\gamma = \frac{E_p(1+\beta\cos\theta_p)}{1-\beta\cos\theta_\gamma+\frac{E_p}{\gamma E_e}(1-\cos\theta_s)}, \tag{1}$$

where E_γ is the energy of the scattered laser photon, E_e is the electron energy, β is the electron velocity relative to the speed of light, θ_p is the incident laser angle, γ is the Lorentz factor of the electron energy, and θ_s is the angle between the incident laser photon and the scattered photon.

Equation (1) indicates that when we limit the scattering angle with a collimator, a narrow bandwidth LCS beam can be generated. The bandwidth of the LCS beam can be described as

$$\frac{\sigma_{E_\gamma}}{E_\gamma} = \sqrt{\left(\frac{\sigma_\theta}{E_\theta}\right)^2+\left(\frac{\sigma_\gamma}{E_\gamma}\right)^2+\left(\frac{\sigma_L}{E_L}\right)^2+\left(\frac{\sigma_\varepsilon}{E_\varepsilon}\right)^2}, \tag{2}$$

where the terms on the right-hand side correspond to the contribution to the bandwidth of the LCS beam from the collimator, the electron energy spread, the laser bandwidth, and the electron beam emittance, respectively [19–21]. Equation (2) indicates that a large energy spread and/or a large emittance of the electron beam cause a wide bandwidth of the LCS beam. However, electron beams circulating in storage rings, where most LCS instruments are developed [1–3,5,6], have small energy spreads ($<10^{-3}$) and low unnormalized emittances (<1 μmrad). Therefore, it is challenging to generate a broad bandwidth LCS beam with a small collimation which is indispensable to obtain a high-resolution image.

We have proposed an F-LCS beam generation by using a helical undulator to excite a circular motion of an electron beam at the electron-laser collision region. The electron beam with a circular motion excited by the helical undulator can have a large beam size and divergence that is expected to broaden the energy spread of the LCS beam. Figure 1 shows a conceptual drawing of the proposed F-LCS beam generation. In the following subsection, we describe our simulation study to confirm the generation of the proposed F-LCS beam.

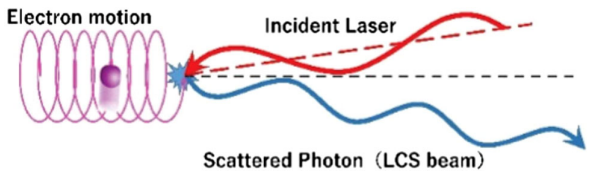

FIG. 1. Conceptual drawing of F-LCS beam generation.

III. EGS5 SIMULATION

The simulation modeling of the proposed F-LCS beam has been developed using the EGS5 code. The electron motion excited by an undulator is expressed as [22]

$$x = -\frac{K_x\lambda_u}{2\pi\gamma}\cos\left(\frac{2\pi}{\lambda_u}z\right) \qquad x' = \frac{K_x}{\gamma}\sin\left(\frac{2\pi}{\lambda_u}z\right)$$
$$y = \frac{K_y\lambda_u}{2\pi\gamma}\sin\left(\frac{2\pi}{\lambda_u}z\right) \qquad y' = \frac{K_y}{\gamma}\cos\left(\frac{2\pi}{\lambda_u}z\right). \tag{3}$$

Here x axis is the horizontal axis, y axis is the vertical axis, and the z axis is the traveling direction of the electron beam in the experimental geometry in UVSOR. In Eq. (3), $K_{x,y}$ are the K values of the helical undulator, λ_u is the undulator period.

The LCS beamline in BL1U of UVSOR (Fig. 2) was assumed for a test experiment. The APPLE-II undulator consists of two helical undulators, which have 20 periods of 8.8 cm, and a 50-cm dispersive section in the middle of APPLE-II was installed at the center of the 6.3-m straight section of the BL1U [16]. It should be noted that the magnetic field of the dispersive section was zero in this calculation as well as in the POP experiment explained in the next section.

Our EGS5 simulation procedure is as follows: First, the transverse electron position and divergence were calculated by Eq. (3) by a random z-position with a Gaussian distribution in the collision region of a size of $\sigma = 45.2$ cm; This size is determined by Rayleigh length of the incident cw laser in the experimental setup. Second, the γ-ray scattering angle was randomly generated to satisfy the probability of Compton backscattering. Then, the energy of each scattered γ ray was calculated one by one. We repeated this routine 10,000,000 times and constructed the energy spectrum.

Figure 3(a) shows the energy distribution of the standard LCS γ ray along the vertical axis (z) after passing through a 2-mmϕ collimator without the undulator ($K = 0$). A position-energy dependency is clearly observed in Fig. 3(a). If we excite the helical undulator with $K = 0.2$,

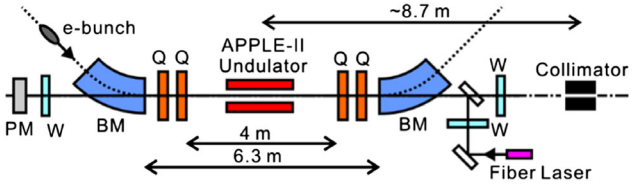

FIG. 2. Schematic drawing of the BL1U beamline in UVSOR. APPLE-II type undulator is installed in 6.3-m straight section. PM: power meter, W: window.

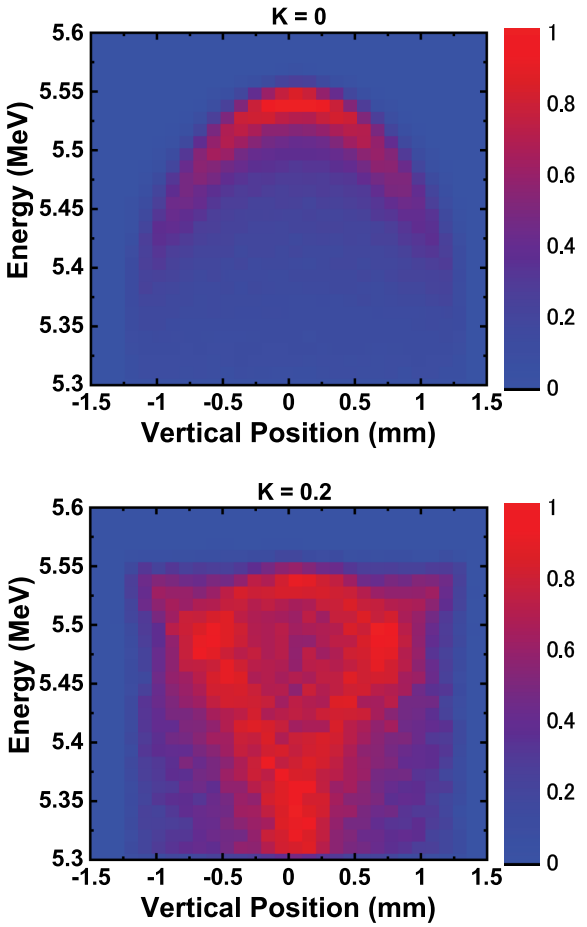

FIG. 3. LCS γ-ray energy distribution in the vertical axis with the undulator K value of (a) $K = 0$, (b) $K = 0.2$.

the position-energy dependency is relaxed as shown in Fig. 3(b). According to Eq. (3), the excited electron beam radius can be calculated to be 1.9 μm with $K = 0.2$ which is negligible to the electron beam size ($\sigma_y = 20$ μm) on the vertical axis and the horizontal axis ($\sigma_x = 580$ μm) in the case of UVSOR. Therefore, the beam divergences excited by the helical undulator are considered to be the main reason for the relaxation of the position-energy dependency in Fig. 3(b). One of the advantages of the LCS beam is its small beam size and small beam divergence. By using Eq. (3) with $K = 0.2$, the electron beam divergence can be calculated to be 132 μrad, which is comparable to the 2-mmϕ collimator defined beam divergence 115 μrad. Therefore, the beam divergence of the F-LCS γ-ray beam will be 175 μrad and the beam size at 1-m downstream of the 2-mmϕ collimator will become 2.35 mmϕ. An applicable K value for the isotope imaging application should be carefully considered. Figure 4 shows the energy spectra of the LCS beams with different K values from 0 to 0.4. As shown in Fig. 4, the wider energy bandwidth is observed with a larger K value. The peak energy shifts to lower energy as the K value becomes larger. The circular motion

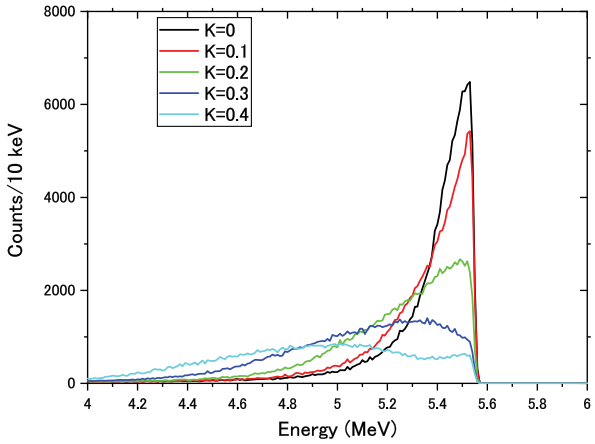

FIG. 4. Energy spectra of the γ-ray beams with different K values from 0 to 0.4.

of the electrons by the helical undulator widens the electron beam size and enlarges the beam divergence. However, the effect of the beam size is small, and the effect of the beam divergence is dominant, as we describe in the above paragraph. According to Eq. (1), for the larger collision angle between the electron beam and the laser, smaller energy of the scattered γ ray should be generated. Therefore, we can observe the peak energy shift at larger K value case in Fig. 4 and Table I which summarizes the simulation results. The energy bandwidth is widened from 2.7% to 22% (FWHM) and the peak energy is shifted from 5.53 to 5.01 MeV by increment of the K value from 0 to 0.4. About 8 times larger bandwidth can be obtained with the collimator diameter of 2 mmϕ. We should mention that the F-LCS beam yield at the top energy region decreases with the increase of the undulator field. In addition, to reconstruct the isotope selective CT image, the transmission γ rays have to be measured [14] and a large K value might not be applicable due to the lack of a clear LCS peak. Therefore, K value of 0.2 would be a suitable for the POP experiment to measure multiple lead isotopes, ^{206}Pb (5.037 MeV) and ^{208}Pb (5.512 MeV), in UVSOR. By using F-LCS beam with $K = 0.2$, the γ-ray flux at 5.087 MeV is about 4 times larger than that with the normal LCS ($K = 0$). On the other hand, the γ-ray flux at 5.512 MeV is about 1.7 times smaller than that with the

TABLE I. Summary of the simulation result.

K value	Peak energy (MeV)	Bandwidth FWHM (%)	Yield (4–5.6 MeV)
0	5.53	2.7	1362
0.1	5.53	3.3	1327
0.2	5.50	7.2	1228
0.3	5.31	14	1082
0.4	5.01	22	914

normal LCS. It should be noted that when we use a F-LCS beam with $K = 0.2$, which has 7.2% FWHM bandwidth, the background γ rays originated from the atomic scattering of the target nuclei should be larger than in the case with the conventional LCS beam. Therefore, a proper detector position and an absorber thickness should be used for the NRF measurement.

IV. EXPERIMENT AT BL1U IN UVSOR

The POP experiment of the F-LCS beam generation was performed at the BL1U in UVSOR. The experimental setup was the same as that shown in Fig. 2 except for the detector system located after the 2-mmϕ collimator made by a 20 cm × 10 cm × 10 cm lead block. The stored electron with an energy of 746 MeV [5] and a current of about 6 mA was used. The laser beam from a Tm-fiber laser system (TLR-50-AC-Y14, IPG Laser GmbH) with around 1 W cw power with random polarization was used for the incident laser beam. The wavelength was 1.896 μm and the spectral linewidth was 0.7 nm. A high-purity germanium (Ge) detector with a relative efficiency of 120% was used for the measurement of the energy spectra of the generated γ rays.

Before the LCS γ-ray generation, we checked the orbit distortion of the stored electron beam by excitation of the undulator with a K value of 0.2. After the orbit correction, the beam position monitor located in BL1U showed that the orbit change was about 25 μm in the horizontal axis and 50 μm in the vertical axis, which is acceptable for the other beamline users.

Figure 5 shows the measured γ-ray beam spectra with K values of 0, 0.1, 0.2, and 0.3. The vertical axis is normalized by the maximum counts in the energy region from 4 to 6 MeV. Although the measured spectra show Ge response, the LCS peak at 5.5 MeV with $K = 0$ gradually disappeared by increasing the undulator K value. The tendency of the peak bandwidth broadening agrees with the EGS5 simulation.

V. DISCUSSION

To verify the simulation result with the experiment, the EGS5 simulation taken into account of the Ge detector response was performed. Figure 6 shows the result of the simulation. The vertical axis is the normalized counts, which was calculated in the same way as Fig. 5. Although the measured energy bandwidth was slightly larger than the simulation result, the simulated LCS spectra well reproduce the experimental results. The slight difference would originate from our simple model assumed for the electron-laser interaction region. We assumed that the electron-laser collision point was the center of the undulator where the 50-cm dispersive section was in the EGS5 simulation. The electron-laser collision point affects the energy spectrum of the collimated LCS beams and is more significant for the F-LCS beam because the circular motion cannot be excited at the dispersive section in our case.

To confirm the effect of the electron-laser collision point, EGS5 simulation has been performed for three collision points, (i) the center of the APPLE-II downstream undulator, (ii) the center of the APPLE-II dispersive section, and (iii) the center of the APPLE-II upstream undulator. The results are shown in Fig. 7. The collision point at the center of the dispersive section, which was the expected point of our experimental condition, has the smallest bandwidth of the F-LCS beam, and those at the upstream and downstream of the undulator sections have wider bandwidths. This suggests that if the electron-laser collision point was shifted to an up or down undulator position, a wider energy bandwidth should be observed. Unfortunately, we could not specify the collision region during the present experiment.

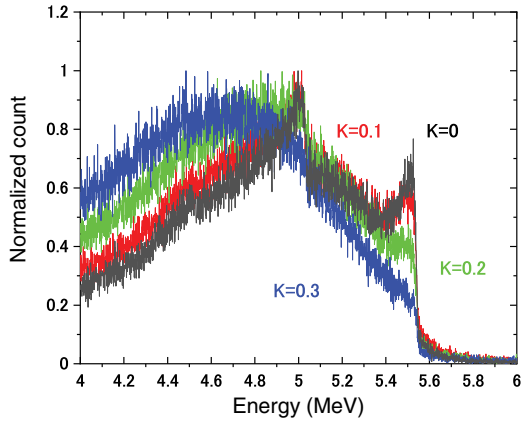

FIG. 5. Measured LCS beam spectra with the undulator K value of 0, 0.1, 0.2, and 0.3. The LCS beam was collimated with 2-mmϕ lead collimator.

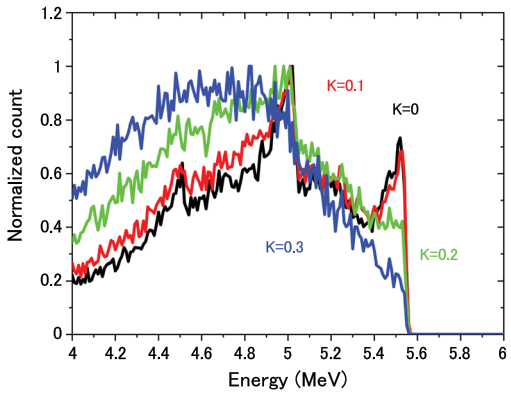

FIG. 6. LCS energy spectra calculated EGS5 including Ge detector response.

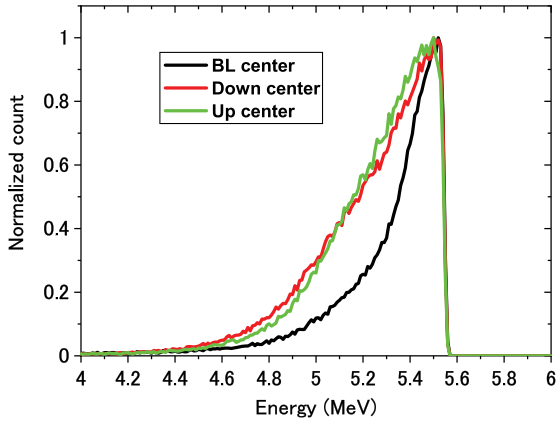

FIG. 7. LCS energy spectra for different collision points calculated EGS5.

VI. CONCLUSIONS

In this paper, we have proposed the generation of F-LCS beams with a broad energy bandwidth and a small beam size using a helical undulator in a storage ring. A simulation study using EGS5 shows the energy bandwidth of the LCS beam with circular motion excited by a helical undulator is widened from 2.7% to 22% (FWHM) with fixed collimator size (2 mmϕ) by varying the undulator K value from 0 to 0.4. The property of the LCS beamline of the BL1U in UVSOR was assumed for the simulation. An experiment of the F-LCS beam generation has been carried out at the BL1U in UVSOR. The APPLE-II undulator was used to generate the circular motion of electron beams. The energy spectra of LCS beams generated with $K = 0$, 0.1, 0.2, and 0.3 have been measured with a Ge detector, and the results agree with the EGS5 simulation. This result supports the successful generation of the F-LCS beam. The spatial distribution of the F-LCS beam, precise modeling of EGS5 simulation, and a multiple NRF excitation experiment should be performed in further study.

ACKNOWLEDGMENTS

This work was supported by the Japanese Sociality for the Promotion of Science (JSPS) KAKENHI under Grant No. 21H01859 and performed at the BL1U of UVSOR Synchrotron Radiation Facility with the approval of Institute for Molecular Science (IMS), National Institute of Natural Science (NINS) (Proposal No. 21-603, 21-806).

[1] H. Ohgaki, T. Noguchi, S. Sugiyama, T. Yama-zaki, T. Mikado, M. Chiwaki, K. Yamada, R. Suzuki, and N. Sei, Linearly polarized photons from Compton backscattering of laser-light for nuclear resonance fluorescence experiments, Nucl. Instrum. Methods Phys. Res., Sect. A **353**, 384 (1994).

[2] H. R. Weller and M. W. Ahmed. The HIγS facility: A free-electron laser generated gamma-ray beam for research in nuclear physics, Mod. Phys. Lett. A **18**, 1569 (2003).

[3] K. Aoki, K. Hosono, T. Hadame, H. Munenaga, K. Kinoshita, M. Toda, S. Amano, S. Miyamoto, T. Mochizuki, M. Aoki, and D. Li, High-energy photon beam production with laser-Compton backscattering, Nucl. Instrum. Methods Phys. Res., Sect. A **516**, 228 (2004).

[4] D. J. Gibson, F. Albert, S. G. Anderson, S. M. Betts, M. J. Messerly, H. H. Phan, V. A. Semenov, M. Y. Shverdin, A. M. Tremaine, F. V. Hartemann, C. W. Siders, D. P. McNabb, and C. P. J. Barty, Design and operation of a tunable MeV-level Compton-scattering-based γ-ray source, Phys. Rev. ST Accel. Beams **13**, 070703 (2010).

[5] H. Zen, Y. Taira, T. Konomi, T. Hayakawa, T. Shi-zuma, J. Yamazaki, T. Kii, H. Toyokawa, M. Katoh, and H. Ohgaki, Generation of high energy gamma-ray by laser Compton scattering of 1.94-μm fiber La-ser in UVSOR-III Electron Storage Ring, Energy Procedia **89**, 335 (2016).

[6] Hong-Wei Wang, Gong-Tao Fan, Long-Xiang Liu, Hang-Hua Xu, Wen-Qing Shen, Yu-Gang Ma, Hiroaki Utsunomiya, Long-Long Song, Xi-Guang Cao, Zi-Rui Hao, Kai-Jie Chen, Sheng Jin, Yu-Xuan Yang, Xin-Rong Hu, Xin-Xiang Li, and Pan Kuang, Commissioning of laser electron gamma beamline SLEGS at SSRF, Nucl. Sci. Tech. **33**, 87 (2022).

[7] W. Bertozzi and R. J. Ledoux, Nuclear resonance fluorescence imaging in non-intrusive cargo inspection, Nucl. Instrum. Methods Phys. Res., Sect. B **241**, 820 (2005).

[8] J. Pruet, D. P. McNabb, C. A. Hagmann, F. V. Hartemann, and C. P. J. Barty, Detecting clandestine material with nuclear resonance fluorescence, J. Appl. Phys. **99**, 123102 (2006).

[9] N. Kikuzawa, R. Hajima, N. Nishimori, E. Minehara, T. Hayakawa, T. Shizuma, H. Toyokawa, and H. Ogaki, Nondestructive detection of heavily shielded materials by using nuclear resonance fluorescence with a laser-Compton scattering γ-ray source, Appl. Phys. Express **2**, 036502 (2009).

[10] I. Daito, H. Ohgaki, G. Suliman, V. Iancu, C. Ur, and M. Iovea, Simulation study on computer tomography imaing of nuclear distribution by quasi monoenergetic gamma rays with nuclear resonance fluorescence: Case study for ELINP application, Energy Procedia **89**, 389 (2016).

[11] H. Zen, H. Ohgaki, Y. Taira, T. Hayakawa, T. Shizuma, I. Daito, J. Yamazaki, T. Kii, H. Toyokawa, and M. Katoh, Demonstration of tomographic imaging of isotope distribution by nuclear resonance fluorescence, AIP Adv. **9**, 035101 (2019).

[12] Hao-Yang Lan, Tan Song, Jia-Lin Zhang, Jian-Liang Zhou, and Wen Luo, Rapid interrogation of special nuclear materials by combining scattering, and transmission nuclear resonance fluorescence spectroscopy, Nucl. Sci. Tech. **32**, 84 (2021).

[13] Haoyang Lan, Tan Song, Zhuhua Luo, Jianliang Zhou, Zhichao Zhu, and Wen Luo, Isotope-sensitive imaging of special nuclear materials using computer tomography based on scattering nuclear resonance fluorescence, Phys. Rev. Appl. **16**, 054048 (2021).

[14] K. Ali, H. Ohgaki, H. Zen, T. Kii, T. Hayakawa, T. Shizuma, H. Toyokawa, Y. Taira, M. Fujimoto, and M. Katoh, Three-dimensional nondestructive isotope-selective tomographic imaging of ^{208}Pb distribution via nuclear resonance fluorescence, Appl. Sci. **11**, 3415 (2021).

[15] T. Hayakawa, H. Ohgaki, T. Shizuma, R. Hajima, N. Kikuzawa, E. Minehara, T. Kii, and H. Toyokawa, Non-destructive detection of hidden chemical compounds with laser Compton-scattering gamma rays, Rev. Sci. Instrum. **80**, 045110 (2009).

[16] M. Adachi, H. Zen, T. Konomi, J. Yamazaki, K. Hayashi, and M. Katoh, Design and construction of UVSOR-III, J. Phys. Conf. Ser. **425**, 042013 (2013).

[17] H. Hirayama, Y. Namito, A. F. Bielajew, S. J. Wilderman, and W. R. Nelson, The EGS5 code system, SLAC Report No. SLAC-R-730 and KEK Report No. 2005–8, 2005.

[18] F. R. Arutyunian and V.A Tumanian, The Compton effect on relativistic electrons and the possibility of obtaining high energy beams, Phys. Lett. **4**, 176 (1963).

[19] C. Curatolo, I. Drebot, V. Petrillo, and L. Serafini, Analytical description of photon beam phase spaces in inverse Compton scattering sources, Phys. Rev. Accel. Beams **20**, 080701 (2017).

[20] N. Ranjan, B. Terzić, G. A. Krafft, V. Petrillo, I. Drebot, and L. Serafini, Simulation of inverse Compton scattering and its implications on the scattered linewidth, Phys. Rev. Accel. Beams **21**, 030701 (2018).

[21] R. Hajima, Bandwidth of a Compton radiation source with an electron beam of asymmetric emittance, Nucl. Instrum. Methods Phys. Res., Sect. A **985**, 164655 (2021).

[22] K. Wille, Introduction to insertion devices, in *Proceedings of the CAS—CERN Accelerator School: Synchrotron Radiation and Free Electron Lasers* (CERN, Geneva, 1998), pp. 61–75.